Electron–phonon coupling and spin fluctuations in 3d and 4d transition metals: implications for superconductivity and its pressure dependence

2009 J. Phys.: Condens. Matter 21 025602

(http://iopscience.iop.org/0953-8984/21/2/025602)

J. Phys.: Condens. Matter **21** (2009) 025602 (13pp) doi:10.1088/0953-8984/21/2/025602

Electron–phonon coupling and spin fluctuations in 3d and 4d transition metals: implications for superconductivity and its pressure dependence

S K Bose

Physics Department, Brock University, St Catharines, ON, L2S 3A1, Canada

Received 6 October 2008, in final form 24 November 2008
Published 11 December 2008
Online at stacks.iop.org/JPhysCM/21/025602

Abstract

We have calculated the electron–phonon coupling for the complete 4d series and the nonmagnetic 3d transition metals using the linear response method and the linear muffin-tin orbitals' basis. A comparison of the linear response results and those obtained via the rigid muffin-tin approximation is provided. Based on the calculated values of the electron–phonon coupling constants, band density of states and the measured values of the electronic specific heat constants, we estimate the spin-fluctuation effects, i.e. the electron–spin-fluctuation (electron–paramagnon) coupling constants in these systems. For the sake of comparison, several other metals, Cu, Zn, Ag, Cd, Al and Pb, are also studied. Alternative estimates of the electron–paramagnon coupling constants are obtained from the values of the Stoner parameters and the band densities of states at the Fermi level. Implications of these results on the superconductivity and its pressure dependence as well as the alloying effects of superconductivity in these systems are discussed. It is pointed out that spin fluctuations play an important role in the validity of the Matthias rule that in metallic systems the optimum conditions for (electron–phonon) superconductivity occur for 5 and 7 valence electrons/atom.

1. Introduction

The electron–phonon (EP) interaction is an important process in solids and the most dramatic manifestation of this interaction is superconductivity in metals, where all of the properties are drastically modified with respect to the normal (non-superconducting) state. In the first approximation the EP coupling constant λ_{ep} can be shown to depend on the electronic density of states at the Fermi level $N(0)$, average phonon frequency $\langle\omega\rangle$ (equivalently, the Debye temperature Θ_D) and the Fermi surface averaged electron–phonon matrix element $\langle I^2\rangle$ [1]. Thus, in many situations, where the other two factors $\langle\omega\rangle$ and $\langle I^2\rangle$ stay more or less unchanged, $N(0)$ alone can decide the variation of the superconducting transition temperature T_c with external conditions. A clear demonstration of this was given by Dynes and Varma [2] for the variation of T_c as a function of defect concentration in A15 compounds and as a function of oxygen concentration in NbO. This result was sometimes interpreted as a rule that λ_{ep} should be proportional to $N(0)$ through the 3d and 4d series of transition metals (see, e.g., Papaconstantopoulos *et al* [3]) and that metals with a large value of $N(0)$ are likely to be superconductors with relatively high T_c. Failure of this simple rule across the 3d and 4d series can be expected on the basis of the fact that the bulk moduli of all transition metals are known to increase (at least initially) as a function of band filling [4, 5] and the bulk moduli of the late transition metals are, in general, higher than those of the early ones. The band filling also has a nontrivial effect on the matrix element $\langle I^2\rangle$. Moreover, an important factor, not figuring in the electron–phonon coupling, is the effect of spin fluctuations. Unlike the electron–phonon coupling, electron–spin-fluctuation (ES) interactions or the electron–paramagnon coupling has a deleterious effect on the spin singlet superconductivity [6, 15], as they lead to breaking of the Cooper pairs. Spin fluctuations are strong in incipient-magnetic materials. In fact, as the d-band filling increases along the 3d series, spin fluctuations become stronger and finally drive Cr and Mn antiferromagnetic and Fe, Co and Ni ferromagnetic. In Pd the effect is believed to be strong enough to suppress superconductivity despite its large

value of $N(0)$ [6, 7]. It is argued that the high value of $N(0)$ in fcc Pd leads to considerable Stoner enhancement of paramagnetic spin susceptibility, making it a borderline ferromagnetic material [7]. The effect of spin fluctuations on the superconductivity for particular 3d and 4d transition metals has been discussed from time to time by various authors, but a systematic study of both EP and ES interactions across the 3d and 4d series has not appeared. In this work we undertake such a study. We have carried out *first-principles* linear response (LR) calculations of the phonon frequencies, electron–phonon coupling and the phonon linewidths using the full potential linear muffin-tin orbitals' (FP-LMTO) method, as implemented by Savrasov and Savrasov [8–10]. Using the calculated values of the band density of states $N(0)$, the electron–phonon coupling constant λ_{ep} and the measured values of the electronic specific heat coefficient γ, we estimate the electron–spin-fluctuation coupling constant λ_{es}. Alternate estimates of λ_{es} are obtained from the calculated values of the Stoner parameter I_s and $N(0)$ or the susceptibility enhancement factor $1/(1 - I_s N(0))$ [6, 11].

Some time back Papaconstantopoulos *et al* [3] presented theoretical results for λ_{ep} for 32 different metals. However, their results were based on the rigid muffin-tin (RMT) approximation of Gaspari and Gyorffy [12]. The shortcomings of this approximation have been discussed by several authors [13]. Our results, calculated from *first principles*, are free of any such approximation, i.e. no shape approximation (muffin-tin or atomic sphere) for the potential is made and the potential changes due to the displacement of the ions are calculated self-consistently. In addition, our discussion includes the effects of the ES interaction, which was neglected in the work of Papaconstantopoulos *et al* [3] In this sense our work can be viewed to complement the above work. We consider 17 metals in total: all nonmagnetic 3d transition metals, all 4d transition metals and, in addition, Cu, Zn, Ag, Cd and Pb. For comparison with the results of Papaconstantopoulos *et al* [3] we also present results based on the rigid atomic sphere approximation within the LMTO scheme. In addition, we calculate the Eliashberg spectral function and compute the superconducting transition temperature T_c by solving the linearized Eliashberg equations near T_c in the imaginary frequency formulation of the problem [14]. Spin-fluctuation effects are included in the solution of the Eliashberg equations following the prescription of Daams *et al* [15] and also by using the McMillan formula.

Understanding the pressure dependence of superconductivity is an important area of condensed matter physics and has been of great interest for a long time [16, 17]. Spin fluctuations are known to be suppressed under pressure. As a result they have a nontrivial effect on the pressure dependence of T_c. Recently the present author [22] has argued that the spin fluctuations in hcp Sc are large and are responsible for complete suppression of superconductivity at normal pressure. It was demonstrated that the suppression of the spin fluctuations combined with the increase in the EP coupling with pressure can account for the observed superconductivity in the high pressure phase of Sc. One of the objectives of the present work is to identify other 3d and 4d metals where spin fluctuations may play a vital role in the pressure dependence of T_c.

Discussion of superconductivity in this work is based on an expression of the Coulomb pseudopotential (see equation (20)), which is derived for simple models by summing a series of many-body (ladder) diagrams [18, 19] under some approximations. It captures the differences between various metals via the valence bandwidth and the maximum phonon frequency, but does not include the spin-fluctuation effects. In a more advanced treatment of superconductivity, as developed recently by Lüders *et al* [20], spin-fluctuation effects may be formally incorporated in a Coulomb pseudopotential that is perhaps nonlocal and spin-dependent. It should be noted that the electron–phonon coupling, based on density functional energy bands, incorporates spin fluctuations in some average sense, as embodied in the exchange–correlation potential [21]. Electron–paramagnon coupling constants discussed in this paper should thus be viewed as estimates of residual spin fluctuations only, suitable for describing relative and qualitative differences between various metals within the scope of conventional (s-wave) superconductivity.

2. Electronic structure and electron–phonon interaction

We use the full potential linear muffin-tin orbitals' (FP-LMTO) and linear response (LR) methods [8–10] to compute the electronic structure, the phonon frequencies, electron–phonon coupling and the phonon linewidths for the ground state crystalline structures of the metals with the experimental values of the lattice parameters [4]. Most calculations employed a two- or three-κ spd LMTO basis for the valence band. Semicore states, whenever appropriate, were treated as valence states in separate energy windows. The charge densities and potentials were represented by spherical harmonics with $l \leqslant 6$ inside the non-overlapping MT spheres and by plane waves with energies $\leqslant$48–70 Ryd, depending on the lattice parameter, in the interstitial region. Dynamical and Hopfield (electron–phonon) matrices were calculated for 40 wavevectors (corresponding to an 8, 8, 6 division) in the irreducible Brillouin zone (BZ) for the hcp metals and for 47 wavevectors (corresponding to a 10, 10, 10 division) for the bcc and fcc metals. Brillouin zone (BZ) integrations involved in obtaining these matrices were performed with the full-cell tetrahedron method [23], using 1200–2000 **k**-points in the irreducible zone. Most results were obtained by using the exchange–correlation potential of Perdew and Wang [24] in the local density approximation. Checks for a couple of cases using GGA1 [25] had revealed similar results.

The EP coupling parameter is often expressed in an approximate form [1] as $\lambda_{ep} = N(0)\langle I^2\rangle/M\langle\omega^2\rangle$. The purely electronic parameter appearing in this relation is the Fermi level DOS $N(0)$. It gives the impression that the coupling parameter is directly proportional to $N(0)$. In fact, the Fermi surface averaged EP matrix element has a complicated dependence on the total as well as partial (angular momentum-resolved) DOSs at the Fermi level. This point will be illustrated in a later discussion. To this end in table 1 we show the Fermi level densities of states for various metals. The basis for the FP-LMTO calculation does not lend itself to a suitable partial-orbital (s-, p-, d-, f-) resolution of the DOSs. This is possible

Table 1. Total FP-LMTO Fermi level DOS $N(0)$ and LMTO-ASA results for total and (approximate) s-, p-, d- and f-orbital-resolved Fermi level DOSs: $\bar{N}(0)$, $\bar{N}_s$, $\bar{N}_p$, $\bar{N}_d$, $\bar{N}_f$. In addition to the 3d and 4d metals, Al and Pb are added for comparison. All DOS are in units of states/(Ryd atom).

Element	Structure	$N(0)$	$\bar{N}(0)$	$\bar{N}_s$	$\bar{N}_p$	$\bar{N}_d$	$\bar{N}_f$
			3d metals				
Sc	hcp	29.0	28.9	0.47	7.42	20.4	0.66
Ti	hcp	12.4	12.4	0.13	2.11	9.81	0.34
V	bcc	25.3	23.6	0.32	3.51	19.2	0.59
Cu	fcc	4.13	4.00	0.56	1.42	1.99	0.03
Zn	hcp	2.73	2.63	0.54	1.65	0.37	0.07
			4d metals				
Y	hcp	26.1	28.0	0.59	7.42	19.2	0.83
Zr	hcp	13.0	13.2	0.19	2.87	9.54	0.58
Nb	bcc	19.9	18.0	0.50	3.52	13.2	0.76
Mo	bcc	8.10	7.69	0.11	1.18	5.98	0.42
Tc	hcp	12.4	12.4	0.22	1.59	10.2	0.43
Ru	hcp	10.9	11.0	0.12	0.74	9.82	0.36
Rh	fcc	17.4	16.8	0.20	0.64	15.7	0.30
Pd	fcc	33.1	31.6	0.30	0.50	30.6	0.19
Ag	fcc	3.63	3.54	0.77	1.70	1.03	0.04
Cd	hcp	3.02	3.04	0.71	1.89	0.35	0.08
Al	fcc	5.45	5.66	1.20	2.61	1.62	0.21
Pb	fcc	6.85	6.73	0.40	5.09	0.99	0.25

in the LMTO-ASA basis which consists of muffin-tin orbitals of pure angular momentum character and no plane waves. In table 1 the partial l-resolved DOSs correspond to LMTO-ASA results, the total DOS for which is also shown.

We have computed both the Eliashberg spectral function:

$$\alpha^2F(\omega) = \frac{1}{N(0)} \sum_{\mathbf{k},\mathbf{k}',ij,\nu} |g^{ij,\nu}_{\mathbf{k},\mathbf{k}'}|^2 \delta(\varepsilon^i_{\mathbf{k}})\delta(\varepsilon^j_{\mathbf{k}'})\delta(\omega-\omega^\nu_{\mathbf{k}-\mathbf{k}'}), \quad (1)$$

and the transport Eliashberg function [10, 14]:

$$\alpha^2_{\rm tr}F(\omega) = \frac{1}{2N(0)\langle v^2_{\rm FS}\rangle} \sum_{\mathbf{k},\mathbf{k}',ij,\nu} |g^{ij,\nu}_{\mathbf{k},\mathbf{k}'}|^2 \times (\vec{v}_{\rm FS}(\mathbf{k}) - \vec{v}_{\rm FS}(\mathbf{k}'))^2\ \delta(\varepsilon^i_{\mathbf{k}})\ \delta(\varepsilon^j_{\mathbf{k}'})\ \delta(\omega-\omega^\nu_{\mathbf{k}-\mathbf{k}'}), \quad (2)$$

where the angular brackets denote the Fermi surface average, $\vec{v}_{\rm FS}$ denotes the Fermi surface velocity and $g^{ij,\nu}_{\mathbf{k},\mathbf{k}'}$ is the electron–phonon matrix element, with ν being the phonon polarization index and $\mathbf{k}, \mathbf{k}'$ representing electron wavevectors with band indices i, and j, respectively. Equation (1) can be written as a BZ sum of the phonon linewidths [26]: $\gamma_{\mathbf{q}\nu}$:

$$\alpha^2F(\omega) = \frac{1}{2\pi N(0)} \sum_{\mathbf{q}\nu} \frac{\gamma_{\mathbf{q}\nu}}{\omega_{\mathbf{q}\nu}} \delta(\omega-\omega_{\mathbf{q}\nu}), \quad (3)$$

with

$$\gamma_{\mathbf{q}\nu} = 2\pi\omega_{\mathbf{q}\nu} \sum_{\mathbf{k},ij} |g^{ij,\nu}_{\mathbf{k},\mathbf{k}+\mathbf{q}}|^2 \delta(\varepsilon^i_{\mathbf{k}})\delta(\varepsilon^j_{\mathbf{k}+\mathbf{q}}). \quad (4)$$

As indicated above, in our calculations the wavevectors $\mathbf{q}$ varied from 40 to 50 within the irreducible BZ, while the wavevectors $\mathbf{k}, \mathbf{k}'$ varied from 1200 to 2000. The EP coupling constant $\lambda_{\rm ep}$ follows from an integral involving the Eliashberg function:

$$\lambda_{\rm ep} = 2\int_0^\infty \frac{{\rm d}\omega}{\omega}\alpha^2(\omega)F(\omega). \quad (5)$$

Table 2. FP-LMTO LR results for the maximum phonon frequency $\omega_{\rm m}$ and average phonon frequencies $\tilde{\omega} = \langle\omega^2\rangle^{1/2}$. $\langle\omega^n\rangle$ and $\omega_{\ln}$ are defined via equations (6) and (7). For comparison, experimental values of the maximum phonon frequencies $\omega_{\rm m}$(exp) and the low temperature limit of the Debye frequencies $\Theta_{\rm D}$ from [4], chapter 5, table 1 are also displayed. All frequency values are in units of meV. $\tilde{\omega}(\Theta_{\rm D}) = \sqrt{\Theta^2_{\rm D}/2}$ is an estimate of $\langle\omega^2\rangle^{1/2}$ obtained from $\Theta_{\rm D}$. The asterisk implies that the value is unavailable.

Element	$\langle\omega\rangle$	$\tilde{\omega}$	$\omega_{\ln}$	$\omega_{\rm m}$	$\omega_{\rm m}$(exp)	$\Theta_{\rm D}$	$\tilde{\omega}(\Theta_{\rm D})$
			3d metals				
Sc	15.2	16.3	13.8	26.6	28.6	31.0	21.9
Ti	19.2	20.5	17.7	33.9	32.0	36.2	25.6
V	20.7	21.8	19.2	32.6	33.1	32.5	23.0
Cu	18.7	19.5	17.8	29.1	29.7	29.5	20.9
Zn	15.0	16.4	13.7	30.8	26.9	28.2	19.9
			4d metals				
Y	11.2	11.6	10.7	17.6	19.2	24.1	17.0
Zr	12.7	13.7	11.6	23.8	22.2	25.1	17.7
Nb	15.6	16.7	14.1	27.4	26.8	23.4	16.6
Mo	23.8	24.3	23.1	33.4	33.1	38.8	27.4
Tc	20.1	20.8	19.4	31.0	26.9–27.5	*	*
Ru	25.1	25.6	24.5	33.7	32.6	51.7	36.6
Rh	22.4	22.8	22.0	30.0	30.0	41.4	29.3
Pd	14.7	15.6	13.7	28.4	27.8	23.6	16.7
Ag	13.3	13.9	12.6	20.6	20.4	19.4	13.7
Cd	5.67	6.92	4.71	18.8	18.6	18.1	12.8
Al	23.8	24.9	22.3	35.4	40.0	36.9	26.1
Pb	5.77	6.23	5.12	9.7	9.3	9.05	6.4

In table 2 we show the maximum phonon frequency $\omega_{\rm m}$ and average phonon frequencies given by the LR calculations. The logarithmically averaged characteristic phonon frequency $\omega_{\ln}$ and the average phonon frequencies $\langle\omega^n\rangle$ are obtained by using the definition given by Allen and Dynes [27]:

$$\omega_{\ln} = \exp\left\{\frac{2}{\lambda_{\rm ep}}\int_0^\infty \frac{{\rm d}\omega}{\omega}\alpha^2(\omega)F(\omega)\ln\omega\right\}. \quad (6)$$

$$\langle\omega^n\rangle = \frac{2}{\lambda_{\rm ep}}\int_0^\infty {\rm d}\omega\,\alpha^2(\omega)F(\omega)\omega^{n-1}, \quad (7)$$

where $\lambda_{\rm ep}$ is defined by equation (5). For comparison we have also tabulated the measured values of the maximum phonon frequencies [28, 29], obtained from inelastic neutron scattering or x-ray diffraction experiments. The experimental values depend on the temperature. In addition, in a few cases the maximum frequencies are not the directly measured values, being obtained, in fact, from a Born–von Karman fit to the measured dispersion relations. The effectiveness of the FP-LMTO linear response method to accurately reproduce the phonon frequencies in various metallic systems has been adequately demonstrated in earlier calculations [9, 10, 30]. In some previous studies (see, e.g., [3]) the mean square phonon frequencies $\langle\omega^2\rangle$ have been estimated from the Debye frequencies $\Theta_{\rm D}$ using relations such as $\langle\omega^2\rangle = \Theta^2_{\rm D}/2$. For a

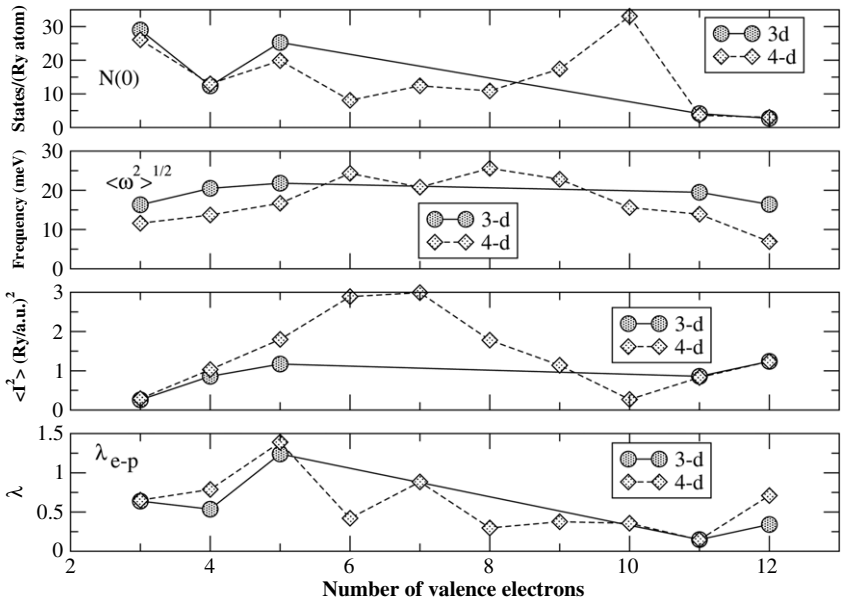

Figure 1. Trends in $N(0)$, $\tilde{\omega} = \langle\omega^2\rangle^{1/2}$, $\langle I^2\rangle$ and λ_{ep} as a function of band filling in 3d and 4d metals.

test of the accuracy of such estimates we have included in the last column of table 2 the quantity $\tilde{\omega}(\Theta_D) = \sqrt{\Theta_D^2/2}$, which can be compared with the LR result $\tilde{\omega} = \langle\omega^2\rangle^{1/2}$. It is clear that the estimate based on Θ_D is usually higher, sometimes by about 30–40%, although for several metals such as Nb, Pd, Ag and Pb it provides surprisingly good results.

In table 3 we show the physical quantities measuring the strength of the electron–phonon interaction. As indicated earlier, the electron–phonon coupling parameter λ_{ep} is a combination of an electronic parameter (Hopfield parameter) $\eta = \langle I^2\rangle N(0)$ ($N(0)$ being the Fermi level DOS for one type of spin) and the mean square phonon frequency $\langle\omega^2\rangle$: $\lambda_{ep} = \eta/m\langle\omega^2\rangle$ [1]. $\langle I^2\rangle$ is the Fermi surface average of the square of the electron–phonon matrix element. The electronic and phonon-related parameters act in opposite directions in affecting the coupling constant: λ_{ep} is enhanced by having higher $\langle I^2\rangle$ at lower frequency. As the Hopfield parameter for transition metals has often been calculated [3] using the rigid muffin-tin approximation of Gaspari and Gyorffy [12], in table 3 we have compared the values obtained via the FP-LMTO LR method (η) and those obtained by using the RMT scheme implemented within the LMTO-ASA method [31, 32], known as the rigid atomic sphere (RAS) method. In table 3 the latter values are labelled as η_{RAS}, while $\langle I^2\rangle_{RAS}$ denotes $\eta_{RAS}/N(0)$.

The trends in the various electronic, phonon and electron–phonon properties are displayed in figure 1. That the electron–phonon coupling parameter λ_{ep} does not have a simple (proportionality) relation to $N(0)$ is clear, Pd being the most prominent example of this. The average frequency (just as the bulk modulus) shows a clear trend: increasing initially with the band filling and then falling beyond half-filling of the band. For metals with more or less similar values of the bulk modulus, the average frequencies for the 4d metals are lower due to larger atomic masses. The Fermi surface average of the electron–phonon matrix element $\langle I^2\rangle$ shows a clear trend for the 4d series: increasing steadily with the band filling, reaching a maximum at half-filling of the 4d band and then falling to a minimum for Pd, when the d band is completely full. It then increases as the 5s band starts filling. One can expect a similar trend in $\langle I^2\rangle$ for the 3d series. Had we included the

Table 3. The Fermi surface averaged square of the electron–phonon matrix element $\langle I^2\rangle$, the Hopfield parameter $\eta = \langle I^2\rangle N(0)$ ($N(0)$ being the Fermi level DOS for one type of spin) and the electron–phonon coupling constant λ_{ep}. For comparison η and $\langle I^2\rangle$ values obtained by using the RMT scheme implemented within the LMTO-ASA method, known as the rigid atomic sphere (RAS) method, are also shown and distinguished from the FP-LMTO LR results via the subscript RAS. $\langle I^2\rangle$ and $\langle I^2\rangle_{RAS}$ are in units of (Ry/bohr)^2, while η and η_{RAS} are in units of Ryd/bohr^2.

Element	$\langle I^2\rangle$	$\langle I^2\rangle_{RAS}$	η	η_{RAS}	λ_{ep}
			3d metals		
Sc	0.0026	0.0030	0.0381	0.0439	0.639
Ti	0.0086	0.0077	0.053 20	0.0478	0.536
V	0.0117	0.0113	0.1476	0.1335	1.24
Cu	0.0086	0.0048	0.0177	0.0096	0.149
Zn	0.0216	0.0040	0.0294	0.0052	0.341
			4d metals		
Y	0.0029	0.0034	0.0382	0.0472	0.652
Zr	0.0103	0.0096	0.0667	0.0636	0.788
Nb	0.0180	0.0170	0.1786	0.1526	1.39
Mo	0.0289	0.0265	0.1170	0.1019	0.421
Tc	0.0299	0.0219	0.1850	0.1357	0.884
Ru	0.0178	0.0224	0.0975	0.1234	0.298
Rh	0.0114	0.0128	0.0994	0.1078	0.377
Pd	0.0027	0.0037	0.0475	0.0581	0.357
Ag	0.0083	0.0032	0.0150	0.0056	0.146
Cd	0.0124	0.0022	0.0188	0.0034	0.710
Al	0.0162	0.0037	0.0442	0.0105	0.535
Pb	0.0150	0.0066	0.0514	0.0224	1.30

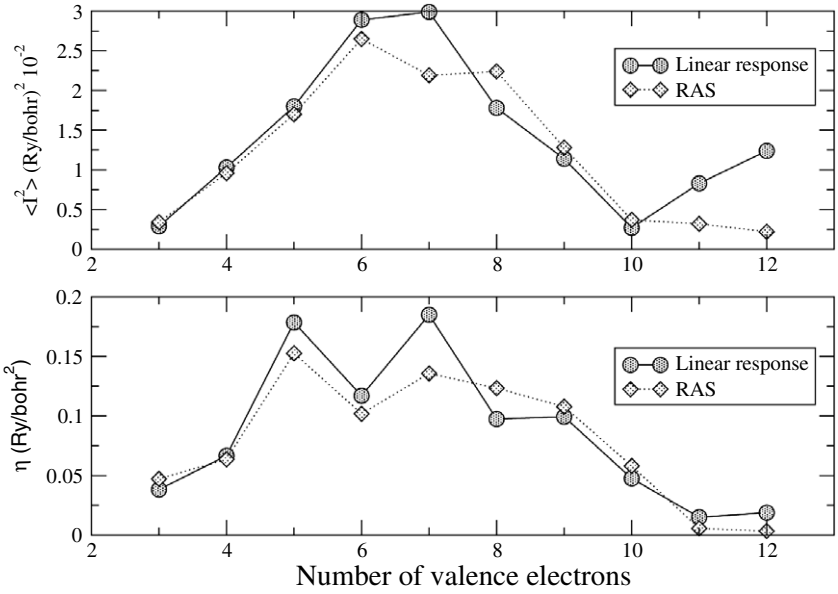

Figure 2. Comparison of the LR results with those based on the RMT approximation of Gaspari and Gyorffy [12].

magnetic 3d metals in their nonmagnetic state in our study, we would be able to see this trend. It is the minimum in $\langle I^2 \rangle$ that is the most dominant factor for Pd in determining its value of λ_{ep}: despite the highest value of $N(0)$ of the metals studied, and an average (i.e. not too high) value of $\langle \omega^2 \rangle$, the electron–phonon coupling parameter is small. This result is in contrast with earlier speculations that the high value of $N(0)$ for Pd should result in a high value of λ_{ep}, leading thus to a surprise in experiments failing to detect superconductivity in Pd down to the lowest temperatures. Note that the results for λ_{ep} clearly point to the validity of the Matthias rule of superconductivity [33], which asserts that for electron–phonon superconductivity in metallic systems the optimum conditions occur for 5 and 7 electrons/atom.

Figure 2 compares the results for 4d metals from LR calculations with those based on the RMT approximation. For d-band metals (both 3d and 4d), i.e. where the Fermi level resides within the d band, the RMT or RAS approximation is reasonably good. Large differences between the LR and RMT results show up for metals where the Fermi level falls in the free-electron (s, p band) part of the spectrum. This is clear from the results shown in table 3 for Cu, Zn, Ag, Cd, Al and Pb. Even for the d-band metals the agreement between the LR and the RAS (or RMT) results is usually good only for normal pressure ground state volumes. Previous studies [34, 35] have revealed increasing disagreement between LR and RMT results with increasing pressure (decreasing volumes).

In figure 3 we display the Eliashberg spectral function for some 3d and 4d transition metals. The first and second rows compare the first three metals from the 3d and 4d series, respectively. The second and third rows compare the first and the middle three metals from the 4d series. In figure 4 we compare the non-transition (free-electron) metals Cu and Zn from the 3d series with their isoelectronic counterparts Ag and Cd from the 4d series. Savrasov [10] has presented the FP-LMTO linear response results for some metals, including Nb, V and Cu, shown in figures 3 and 4. The results shown for the other 10 metals have not appeared in the literature. Our results for Nb, V and Cu are in good agreement with those of Savrasov [10]. Small differences might be there due to different choices of the exchange–correlation potentials, the number of plane waves and the number of phonon wavevectors for which the dynamical and Hopfield matrices are computed. The Eliashberg spectral functions for all of these metals follow closely their phonon density of states, indicating that no unusually large coupling to electron states arises from particular parts of the phonon spectra. Phonon densities of states are available in [28]

Figures 5 and 6 illustrate to what extent an attempt to understand the strength of the electron–phonon interaction, based solely on the consideration of the total and partial densities of electron states, might (not) work. It is clear from the example of Pd discussed above that a high value of $N(0)$ does not guarantee a high value of the Hopfield parameter η. Contrary to a popular and often used conjecture, a high value of d-orbital projected Fermi level DOS $N_d(0)$ is also not a good indicator. As revealed by table 1, the ratio $N_d/N(0)$ increases monotonically with band filling across the 4d series, while the Hopfield parameter shows a complicated non-monotonic behaviour (figure 2). The Gaspari and Gyorffy [12] RMT expression for the Hopfield parameter η shows the dependence on total and partial electronic DOSs at the Fermi level and it is not a simple one. Within the RMT the spherically averaged part of the Hopfield parameter is obtained from [12]

$$\eta = 2N(0) \sum_l (l+1) M_{l,l+1}^2 \frac{f_l}{2l+1} \frac{f_{l+1}}{2l+3}, \tag{8}$$

where $N(0)$ is the Fermi level DOS per atom per spin and f_l is a relative partial state density:

$$f_l = \frac{N_l(0)}{N(0)}. \tag{9}$$

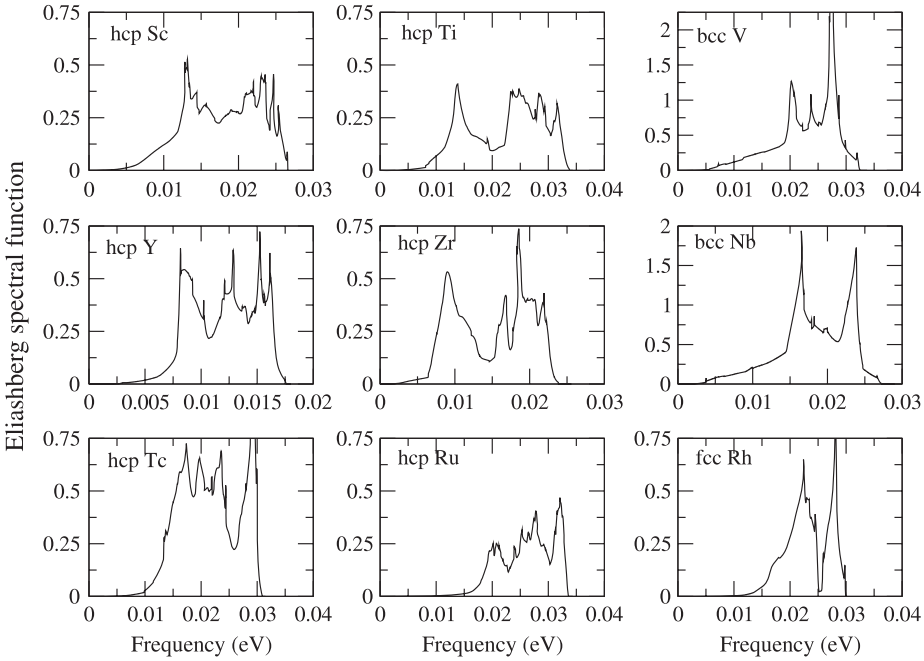

Figure 3. Eliashberg spectral function $\alpha^2 F(\omega)$ as a function of the frequency ω from some 3d and 4d transition metals.

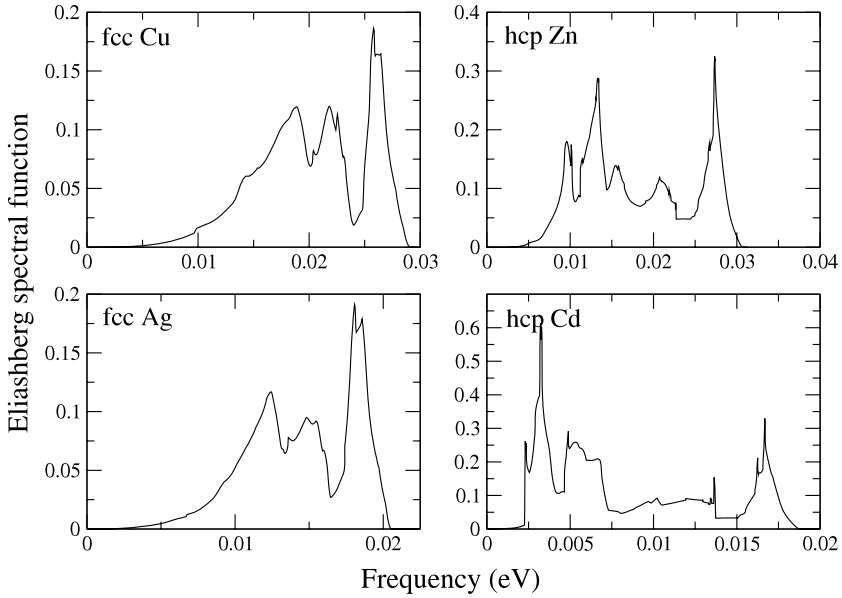

Figure 4. Eliashberg spectral function $\alpha^2 F(\omega)$ as a function of the frequency ω for non-transition (free-electron) 3d metals Cu and Zn and their isoelectronic 4d counterparts Ag and Cd.

$M_{l,l+1}$ is the electron–phonon matrix element obtained from the gradient of the one-electron potential $V(r)$ and the radial solutions R_l and R_{l+1} of the Schrödinger equation within the muffin-tin sphere of radius S evaluated at the Fermi energy:

$$M_{l,l+1} = \int_0^S R_l \frac{\mathrm{d}V}{\mathrm{d}r} R_{l+1} r^2 \,\mathrm{d}r. \tag{10}$$

In LMTO-ASA S stands for the radius of the space filling and volume-preserving (and hence slightly overlapping) atomic spheres. If it were possible to neglect the matrix elements $M^2_{l,l+1}$ and all partial DOSs other than $N_\mathrm{d}(0)$, a proportionality of η to fractional d-DOS, $N_\mathrm{d}(0)/N(0)$ could be expected. In fact, the dependence would be on the product $N_\mathrm{p}(0)N_\mathrm{d}(0)/N(0)^2$, if the contributions from the s–p and d–f scattering were neglected. It is not clear to what extent this ratio alone would correctly reflect the variation of η across the 3d or 4d transition metal series. To explore this, in figure 5 we have plotted the following combinations of the DOS ratios for 4d metals:

$$N_1 = \left(N_\mathrm{s}N_\mathrm{p} + \tfrac{2}{15}N_\mathrm{p}N_\mathrm{d} + \tfrac{3}{35}N_\mathrm{d}N_\mathrm{f}\right)/N(0) \tag{11}$$

$$N_2 = \left(\tfrac{2}{15}N_\mathrm{p}N_\mathrm{d} + \tfrac{3}{35}N_\mathrm{d}N_\mathrm{f}\right)/N(0) \tag{12}$$

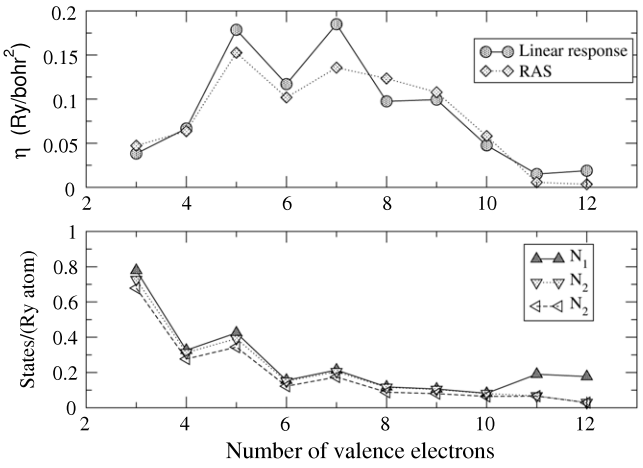

Figure 5. The Hopfield parameter η for 4d metals calculated via the LR method and the RAS (upper panel) approximation, and the DOS combinations $N_1 - N_3$ (see the text for details) in the RMT expression (8) that might be used to represent the Hopfield parameter (lower panel).

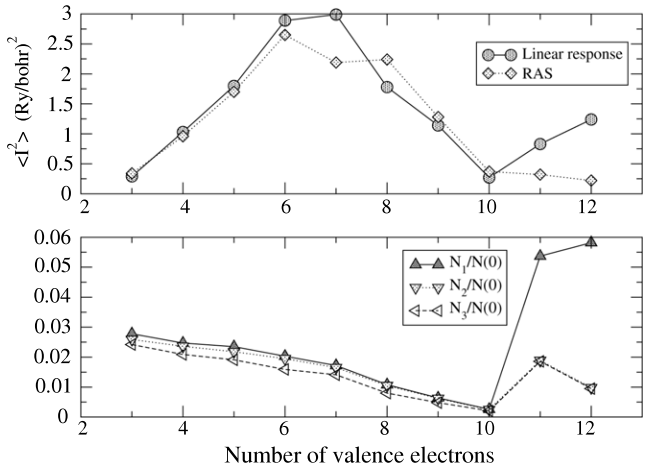

Figure 6. Fermi surface average of the electron–phonon matrix element $\langle I^2 \rangle$ for 4d metals obtained via linear response method and the RAS approximation (upper panel), and the DOS combinations $N_1/N(0) - N_3/N(0)$ (see the text for details) in the RMT expression (8) that might be used to represent $\langle I^2 \rangle$ (lower panel).

$$N_3 = \left(\tfrac{2}{15} N_\mathrm{p} N_\mathrm{d}\right) / N(0), \tag{13}$$

to represent the DOS dependence of the Hopfield parameter and compared them with the actual LR and RMT(RAS) values of η. All partial DOSs are taken at the Fermi level.

In figure 6 we plot the DOS combinations $N_1 - N_3$ divided by $N(0)$ to represent the DOS dependence of $\langle I^2 \rangle$ and compare them with the actual LR and RMT/RAS values. It is clear from figures 5 and 6 that the matrix elements $M^2_{l,l+1}$ play a vital role in deciding the strength of η and $\langle I^2 \rangle$ and cannot be neglected. Hence, statements associating large DOSs such as N_d or $N(0)$ with large electron–phonon coupling must be considered with caution and be backed by supplementary arguments. A large $N(0)$ or N_d does not guarantee a large Hopfield parameter, and definitely not λ_ep, which is further dependent on the phonon frequencies. The importance of the s–p scattering for the non-transition metals Zn and Cd can be clearly seen in figures 5 and 6. In fact, the s–p channel provides the largest contribution to η and $\langle I^2 \rangle$ for these metals, while the contribution from the d–f channel can be safely neglected.

3. Superconducting transition temperature T_c

The superconducting transition temperature can be obtained by solving the linearized isotropic Eliashberg equation at T_c (see, e.g., [14]):

$$\begin{aligned} Z(\mathrm{i}\omega_n) &= 1 + \frac{\pi T_\mathrm{c}}{\omega_n} \sum_{n'} W_+(n-n')\mathrm{sgn}(\omega_{n'}), \\ Z(\mathrm{i}\omega_n)\Delta(\mathrm{i}\omega_n) &= \pi T_\mathrm{c} \sum_{n'}^{|\omega_n| \ll \omega_\mathrm{c}} W_-(n-n') \frac{\Delta(\mathrm{i}\omega_{n'})}{|\omega_{n'}|}, \end{aligned} \tag{14}$$

where $\omega_n = \pi T_\mathrm{c}(2n+1)$ is a Matsubara frequency, $\Delta(\mathrm{i}\omega_n)$ is an order parameter and $Z(\mathrm{i}\omega_n)$ is a renormalization factor. Interactions W_+ and W_- contain a phonon contribution λ_ep, a contribution from spin fluctuations λ_es and effects of scattering from impurities. With scattering rates $\gamma_\mathrm{m} = \frac{1}{2\tau_\mathrm{m}}$ and $\gamma_\mathrm{nm} = \frac{1}{2\tau_\mathrm{nm}}$ referring to magnetic and nonmagnetic impurities, respectively, the expressions for the interaction terms are

$$W_+(n-n') = \lambda_\mathrm{ep}(n-n') + \lambda_\mathrm{es}(n-n') + \delta_{nn'}(\gamma_\mathrm{nm} + \gamma_\mathrm{m}), \tag{15}$$

and

$$\begin{aligned} W_-(n-n') &= \lambda_\mathrm{ep}(n-n') - \lambda_\mathrm{es}(n-n') \\ &\quad - \mu^*(\omega_\mathrm{c}) + \delta_{nn'}(\gamma_\mathrm{nm} - \gamma_\mathrm{m}). \end{aligned} \tag{16}$$

The phonon contribution is given by

$$\lambda_\mathrm{ep}(n-n') = 2\int_0^\infty \frac{\mathrm{d}\omega\, \omega \alpha^2(\omega) F(\omega)}{(\omega_n - \omega_{n'})^2 + \omega^2}, \tag{17}$$

where $\alpha^2(\omega)F(\omega)$ is the Eliashberg spectral function, defined by equation (1). $\lambda_\mathrm{ep}(0) = \lambda_\mathrm{ep}$ is the electron–phonon coupling parameter, the values of which are given in table 3. The contribution connected with spin fluctuation can be written as

$$\lambda_\mathrm{es}(n-n') = \int_0^\infty \frac{\mathrm{d}\omega^2 P(\omega)}{(\omega_n - \omega_{n'})^2 + \omega^2}, \tag{18}$$

where $P(\omega)$ is the spectral function of spin fluctuations, related to the imaginary part of the transversal spin susceptibility $\chi_\pm(\omega)$ as

$$P(\omega) = -\frac{1}{\pi} \left\langle |g_{\mathbf{k}\mathbf{k}'}|^2 \,\mathrm{Im}\, \chi_\pm(\mathbf{k}, \mathbf{k}', \omega) \right\rangle_\mathrm{FS}, \tag{19}$$

where $\langle\ \rangle_\mathrm{FS}$ denotes the Fermi surface average. $\lambda_\mathrm{es} = \lambda_\mathrm{es}(0)$ is often referred to as the electron–spin-fluctuation or electron–paramagnon coupling constant.

In equation (16), $\mu^*(\omega_\mathrm{c})$ is the screened Coulomb interaction:

$$\mu^*(\omega_\mathrm{c}) = \frac{\mu}{1 + \mu \ln(E/\omega_\mathrm{c})}, \tag{20}$$

with $\mu = \langle N(0) V_\mathrm{c} \rangle_\mathrm{FS}$ being the Fermi surface average of the Coulomb interaction. E is a characteristic electron energy,

usually chosen as the Fermi energy E_F and ω_c is a cutoff frequency, usually chosen ten times the maximum phonon frequency: $\omega_c \simeq 10\omega_{ph}^{max}$.

For a start, we ignore all consideration of spin fluctuations and impurity scattering and solve the Eliashberg equation with only the electron–phonon term and the Coulomb pseudopotential $\mu^*(\omega_c)$. As is often done, we assume that a reasonable value for μ is ∼1.0, and from the calculated Fermi energies E_F we obtain μ^* for all the metals, with the cutoff frequency ω_c assumed to be ten times the maximum phonon frequency. The Eliashberg equations (14) can be solved iteratively from the knowledge of the Eliashberg spectral function. The critical temperature can be identified by the opening of the gap in the electronic spectrum, which means a non-vanishing order parameter Δ. One way to calculate the critical temperature is to assume that at or close to T_c the square of the gap function, being close to zero, can be neglected. This converts the problem into the solution of a simple eigenvalue problem, with T_c being the highest temperature at which the largest eigenvalue is unity. There are efficient algorithms, e.g. the power method, that can be used to calculate the largest eigenvalue and the corresponding eigenvector. The values of $\mu^*(\omega_c)$ and T_c are listed in table 4, where we have omitted the metals for which both calculated and experimental values of T_c are zero. Note that T_c values are dependent on $\mu^*(\omega_c)$ and equation (20) is expected to provide only a reasonable estimate. In fact, $\mu^*(\omega_c)$ is strictly unknown. Therefore, in table 4 in a few cases (where spin fluctuations are not expected to be large) we have noted values of $\mu^*(\omega_c)$, which would yield values of T_c close to the experimental values. The other unknown in the problem is, of course, the electron–paramagnon coupling constant λ_{es}, which we discuss in section 4.

For pedagogical reasons, we have listed in table 3 the values of T_c obtained by using the Allen–Dynes form [14] of the McMillan expression:

$$T_c = \frac{\omega_{ln}}{1.2} \exp\left\{-\frac{1.04\,(1+\lambda_{ep})}{\lambda_{ep} - \mu^*(1+0.62\lambda_{ep})}\right\}, \qquad (21)$$

where ω_{ln} is the logarithmically averaged phonon frequency [14], obtained from our LR calculations and reported in table 2. Note that the Coulomb pseudopotential μ^* appearing in the McMillan equation above is related to $\mu^*(\omega_c)$ appearing in the Eliashberg equation via [14]

$$\mu^* = \mu^*(\omega_{ln}) = \frac{\mu^*(\omega_c)}{(1+\mu^*(\omega_c)\ln(\omega_c/\omega_m))}. \qquad (22)$$

Our results are computed with $\omega_c/\omega_m = 10$. The T_c values obtained by solving the Eliashberg equations and those from the McMillan expression equation (21) show excellent agreement. This shows that the analytic expression represents very well the solution of the Eliashberg equation, when the same $\alpha^2F(\omega)$ function which is used in the Eliashberg equation is used to compute the quantities ω_{ln} and λ_{ep} for the McMillan equation. The results also lend credence to the correspondence between $\mu^*(\omega_c)$ and μ^* given by equation (22). In practice, the McMillan equation is used to estimate λ_{ep} from measured values of T_c and errors result from uncertainties in the values of ω_{ln} and μ^*. It should be noted that calculations for hcp Fe under pressure [34] had shown the McMillan expression to overestimate T_c with respect to the results from the Eliashberg equation, while for fcc and bct boron (extreme high pressure phases) an opposite trend was revealed [35]. It is possible that the validity of the McMillan expression is somewhat restricted to metals close to their ground state densities.

Table 4. The Coulomb pseudopotential $\mu^*(\omega_c)$, superconducting transition temperature T_c from the solution of the Eliashberg equation, Coulomb pseudopotential μ^* for use in the McMillan equation (21), the transition temperature T_c^M obtained from the McMillan equation and the measured values of the transition temperatures T_c(exp) (table 1, chapter 12 of [4] and [36]). Metals for which both experimental and calculated values of T_c are zero have been omitted. The results do not include spin-fluctuation effects. In a couple of cases where spin fluctuations are expected to be negligible, we show $\mu^*(\omega_c)$ values that would yield T_c s in agreement with the measured values T_c(exp).

Element	$\mu^*(\omega_c)$	T_c (K)	μ^*	T_c^M (K)	T_c(exp) (K)
			3d metals		
Sc	0.2528	2.17	0.1598	2.21	<0.1
Ti	0.2563	1.19	0.1612	1.19	0.39
V	0.2500	17.35	0.1586	16.37	5.38
Zn	0.2358	0.0	0.1528	0.02	0.875
	0.06	0.8			
			4d metals		
Y	0.2333	2.20	0.1518	2.06	0.0
Zr	0.2389	3.95	0.1541	4.01	0.546
Nb	0.2400	15.6	0.1500	14.6	9.50
Mo	0.2451	0.35	0.1567	0.30	0.92
Tc	0.2400	9.26	0.1546	8.98	7.7
Ru	0.2398	0.0	0.1545	0.002	0.51
	0.08	0.5			
Rh	0.2326	0.0	0.1515	0.11	0.0003
Cd	0.2016	1.53	0.1377	1.41	0.56
Al	0.2250	1.93	0.1482	1.90	1.14
Pb	0.1700	6.02	0.1200	5.44	7.193

4. Spin fluctuations and electron paramagnon coupling

Spin fluctuations are supposed to be large for metals that are borderline magnetic, i.e. exhibit what is known as incipient magnetism. Such systems are characterized by large exchange–correlation enhancement of static spin susceptibility χ. The enhancement factor with respect to the Pauli spin susceptibility χ_0 can be put in the form $\chi/\chi_0 = 1/(1-I_sN(0))$, where I_s is an exchange–correlation-dependent integral [37] and can be identified with the Stoner parameter in the Stoner model, which assumes a wavevector-independent exchange splitting of the paramagnetic electron bands to describe the ferromagnetic state.

For a proper theoretical treatment of the spin-fluctuation effects one needs to compute $\lambda_{es}(n-n')$ from the spin susceptibility function given by equation (18). However, it is important to note that such treatments tacitly assume a Migdal-like theorem being applicable to spin fluctuations.

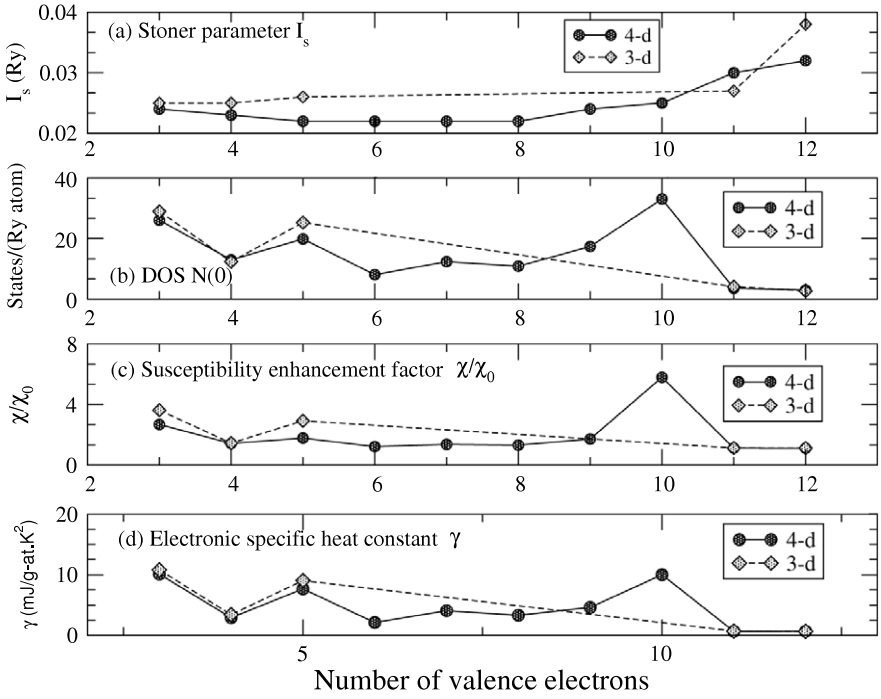

Figure 7. Correlation between the low temperature electronic specific heat coefficient γ and the spin susceptibility enhancement factor χ/χ_0. γ is given in units of mJ/g-at.K^2 [38].

The Eliashberg equations (equation (14)) are based on the assumption that the maximum or the cutoff energy of spin fluctuation is much smaller than the characteristic electronic energy, e.g. the Fermi level.

A somewhat qualitative treatment of spin fluctuations can be based on estimating $\lambda_{es} = \lambda_{es}(0)$ from experiments. Both electron–phonon and the electron–paramagnon interactions contribute to the electronic specific heat. In an independent one-electron picture this is interpreted as the electronic mass enhancement or, equivalently, the enhancement of the density of states over the bare band value $N(0)$. The latter is the value given by calculations, where these interactions are not included in the one-electron Hamiltonian. Thus, an estimate of the electron–paramagnon coupling constant λ_{es} can be obtained from the measured value of the temperature coefficient of the electronic specific heat γ, and the calculated values of the bare band density of states and the electron–phonon coupling constant λ_{ep}:

$$\gamma = \frac{\pi^2}{3} k_B^2 N^*(0) \tag{23}$$

$$N^*(0) = N(0)(1 + \lambda_{\text{eff}}) \tag{24}$$

$$\lambda_{\text{eff}} = \lambda_{ep} + \lambda_{es}. \tag{25}$$

Here, γ and $N(0)$ refer to the values per atom. The Coulomb interactions are included, in an average sense, in the density functional calculations of $N(0)$ and have therefore been left out of equation (23). Specific heat enhancement due to electron–paramagnon coupling should be pronounced for systems with large exchange enhancement of spin susceptibility. In figure 7 we display the bare band densities of states, the Stoner parameters I_s [37], susceptibility enhancement factors χ/χ_0 and electronic specific heat constants γ [38] for the 3d and 4d metals studied. A strong correlation between γ and χ/χ_0 is noticeable.

Values of λ_{es} obtained by using equation (23) are shown in table 5 as $\lambda_{es}^{(1)}$. The difficulty with using equation (23) is that it can only be used as a guide. As discussed by MacDonald [21], spin density functional calculations include partly the spin-fluctuation effects via the exchange–correlation potential. As noted by Savrasov and Savrasov [10], the use of equation (23) may result in negative values of λ_{es}, indicating that the value of $N(0)$ in this equation needs to be reduced with respect to the value obtained from the spin density functional calculation. Dynes and Varma [2] use equation (23) with an adjustable prefactor on the right-hand side. This prefactor is less than unity, but unknown. In table 5 we have left blank the values of $\lambda_{es}^{(1)}$, whenever it comes out to be negative via the use of equation (23). For an alternate estimate of λ_{es}, we follow the analysis presented in [34] (see also [40]). An integration of $P(\omega)$ given by equation (19), under some approximations, leads to the result

$$\lambda_{es} = \alpha N(0) I_s \ln \frac{1}{1 - N(0) I_s}, \tag{26}$$

where the constant α is of the order of unity ($\leqslant 1$)). In [34], where an analysis for hcp Fe was presented for varying volumes per atom, the constant α was chosen by a fit to the measured T_c at a given pressure. Here we choose $\alpha = 1$ and provide the corresponding estimates of λ_{es} in table 5 as $\lambda_{es}^{(2)}$, which should be considered as the upper limits to the values of λ_{es} coming from equation (26).

The two methods yield different estimates of λ_{es}, with some common features. Both Sc and Y, the first transition

Table 5. Values of electron–paramagnon coupling constants from electronic specific $\lambda_{es}^{(1)}$ and from equation (26) $\lambda_{es}^{(2)}$.

Element	$\lambda_{es}^{(1)}$	$\lambda_{es}^{(2)}$
3d metals		
Sc	0.513	0.465
Ti	0.005	0.06
V		0.35
Zn	0.020	0.006
4d metals		
Y	0.579	0.309
Zr		0.053
Nb		0.126
Mo	0.078	0.017
Tc	0.012	0.043
Ru	0.441	0.033
Rh	0.145	0.114
Pd	0.256	0.73
Cd		0.005
Al		0.034

Table 6. Coulomb pseudopotential μ^* for use in the McMillan equation (27), electron–paramagnon coupling constant λ_{es}, the transition temperature T_c^M obtained from the McMillan equation (21) without the inclusion of spin fluctuations, the transition temperature $T_c^M(SF)$ from equation (27) and the measured values of the transition temperatures $T_c(exp)$. The choice of μ^* and λ_{es} was guided by the values in tables 4 and 5, while λ_{ep} and ω_{ln} are strictly the calculated values.

Element	μ^*	λ_{es}	T_c^M (K)	T_c^M(SF) (K)	T_c(exp) (K)
3d metals					
Sc	0.160	0.465	2.21	0.0	<0.1
Ti	0.161	0.06	1.19	0.30	0.39
V	0.140	0.25	16.4	5.0	5.38
4d metals					
Y	0.152	0.309	2.06	0.0	0.0
Zr	0.250	0.053	3.95	0.51	0.546
Nb	0.130	0.126	14.6	9.0	9.50
Tc	0.155	0.043	8.98	6.6	7.7
Cd	0.200	0.005	1.41	0.63	0.56

metals from the 3d and 4d series, show large values of λ_{es}, irrespective of the method used, and so does Pd. In addition, Ru and Rh from the 4d series are likely candidates for moderately large λ_{es}, while other metals whose superconducting properties are quite possibly affected by spin fluctuations are Ti, V, Nb, Mo and Tc. Rietschel and Winter [39] have discussed spin fluctuations in Nb and V, based on specific heat, susceptibility and reasonable models of the spectral function $P(\omega)$ in equations (16) and (19). Their values of 0.21 and 0.34 for Nb and V, respectively, compare well with our values of 0.13 and 0.35. The values of λ_{es} for Sc and Y are large enough to render them non-superconducting. Without the spin-fluctuation effects they both would be superconducting with similar values of T_c. Contrary to the popular belief that Pd would be superconducting in the absence of spin fluctuations, it transpires that the electron–phonon coupling in Pd is sufficiently low to render it non-superconducting even without considerations of spin fluctuations. Pb and Al are simple metals, and as such spin fluctuations are expected to have negligible effects in these cases. The calculated values of T_c for them without any consideration of spin fluctuations are in excellent agreement with the measured values (table 4).

Daams *et al* [15] have suggested that the effects of spin fluctuations on T_c can be incorporated by a simple rescaling of λ_{ep} and the Coulomb pseudopotential μ^* in the Eliashberg equations: $\lambda_{ep} \to \lambda_{ep}/(1+\lambda_{es})$, $\mu^* \to (\mu^* + \lambda_{es})/(1+\lambda_{es})$. The underlying assumption is that in the range of the phonon frequencies the susceptibility $\chi_{\pm}(\omega)$ in equation (19) is essentially static and the peak in the spectral function $P(\omega)$ occurs at a frequency far above the maximum phonon frequency. We have solved the Eliashberg equations by dropping explicitly the terms $\lambda_{es}(n-n')$ in equations (15) and (16), while rescaling λ_{ep} and μ^* as indicated above. Alternatively, we use an extension of the McMillan formula [40] that is often used to incorporate the spin-fluctuation effects:

$$T_c = \frac{\omega_{ln}}{1.2} \exp\left\{-\frac{1.04(1+\lambda_{ep}+\lambda_{es})}{\lambda_{ep}-\lambda_{es}-\mu^*[1+0.62(\lambda_{ep}+\lambda_{es})]}\right\}. \quad (27)$$

Here $\mu^* = \mu^*(\omega_{ln})$, as listed in table 4. This formula is meaningful as long as λ_{es} is sufficiently less than λ_{ep}, so that the denominator in the argument of the exponential in equation (27) stays positive and not close to zero. The two treatments yield similar results. Since the values of λ_{es} are not rigorously derived, we quote some results based on equation (27).

With the inclusion of λ_{es} both Sc and Y show a $T_c \sim 0$ K. For Nb $\lambda_{es} = 0.126$ and $\mu^* = 0.15$ would reduce T_c to 8 K, in excellent agreement with the measured value 9.5 K. Lowering μ^* to 0.13 results in almost exact agreement with the measured value of T_c. In table 6 we display the effect of including the spin fluctuations on the calculated T_c based on equation (27). The values of ω_{ln} and λ_{ep} have been kept strictly the same as the calculated values (tables 2 and 3). The choice of μ^* and λ_{es} has been guided by the values in tables 4 and 5 to obtain agreement with the measured values of T_c. The closeness of these values to the values in tables 4 and 5 lend credibility to our analysis. An attempt to exactly fit the measured T_c was not done, as the goal of the exercise is to show that reasonable choices of μ^* and λ_{es}, consistent with the values in tables 4 and 5, are able to explain the measured values of T_c.

That Sc should be superconducting was a conclusion reached by Papaconstantopoulos *et al* [3] on the basis of their RMT calculation of λ_{ep}. However, they had considered Sc in a bcc structure and surmised that the calculation for the hcp phase would yield a lower λ_{ep}, which would explain why superconductivity has not been seen in hcp Sc down to 0.1 K [36]. Our results show that, on the basis of λ_{ep} alone, hcp Sc should be superconducting and that it is the large spin fluctuations leading to breaking of the Cooper pairs that is responsible for the absence of superconductivity in this case. In fact, they quote two possible values of λ_{ep}, 0.639 and 0.489.

The latter value is obtained when the d–f channel contribution is reduced by 50% (see [3] for details), while the former coincides exactly with our FP-LMTO linear response result for the hcp phase. Although their RMT results for $\langle I^2 \rangle$ are close to our linear response results for the transition metals, there are significant differences for simple and noble metals Al, Cu, Zn, Ag, Cd and Pb. In addition, their estimation of the average phonon frequency based on the Debye temperature suffers from inaccuracies, as shown in table 2. This explains why they do not find superconductivity for Al, while experiments and our linear response results indicate otherwise, and why their calculated T_c for technetium is considerably lower than the experimental value of 7.73 K.

Large spin fluctuations and the nature of incipient magnetism in hcp Sc have been discussed by several authors [41–46]. Thakor *et al* [44] and Crowe *et al* [47] have discussed spin susceptibility in Y and its similarity to that in Sc. For a detailed discussion of the comparison of spin-fluctuation effects in hcp Sc and fcc Pd readers are directed to [22]. Ru and Rh, with moderately large λ_{es} in table 5, are known to show magnetic or borderline magnetic behaviour under conditions of low coordination and/or higher volume per atom. Ru monolayers on noble metal surfaces have been found to be magnetic, while V, Ru, Rh and Pd show induced magnetization, when in contact with ferromagnetic materials [48]. Ru monolayers, epitaxially adsorbed on graphite, have been found to be ferromagnetic at temperatures below 250 K [49, 50]. This result is supported by theoretical studies as well [51]. Table 4 shows that no electron–paramagnon coupling is needed to explain the low T_c of Ru and the absence of superconductivity in Rh, the calculated T_c without electron–paramagnon coupling for both being zero. However, it is possible that in these cases $\mu^*(\omega_c)$ is overestimated and/or λ_{ep} is undervalued, leaving room for spin fluctuations to indeed play some role after all. A similar comment might apply to Mo.

5. Pressure dependence of T_c and alloying effects

Spin fluctuations, like all other correlation effects, are supposed to be reduced under increasing pressure. In [22] it was argued that the increase in λ_{ep} with pressure in hcp Sc, together with the suppression of spin fluctuations, strongly supports the appearance of superconductivity in the high pressure complex Sc-II phase and subsequent increase of T_c under pressure, observed recently by Hamlin and Schilling [52]. Similar considerations must hold for the pressure dependence of T_c in yttrium as well. Hamlin *et al* [53] have reported that Y becomes superconducting under high pressure, with $T_c = 17$ K at 89 GPa and 19.5 K at 115 GPa of pressure. Yin *et al* [54] have studied the pressure dependence of T_c in the fcc phase of Y. Yttrium undergoes a series of phase changes under pressure: hcp → Sm-type → dhcp → dfcc (distorted fcc with trigonal symmetry), at pressures around 12 GPa, 25 GPa and 3–35 GPa, respectively. The analysis by Yin *et al* [54] for the fcc phase does not consider spin-fluctuation effects. Our results indicate that the suppression of spin fluctuations should play an important role in the appearance of superconductivity in Y under pressure, as well as the increase in T_c with pressure. Incidentally, there may be non-negligible differences due to the crystal structure as well. As we show in figure 8, there is a significant difference between the phonon densities of states of the hcp and fcc (studied by Yin *et al* [54]) phases of yttrium. Under pressure, considerable changes in the phonon density of states takes place, along with a broadening of the entire spectrum, as found by these authors. Apart from Sc and Y, spin-fluctuation effects should also be relevant for elements such as Nb and V as well as alloys containing Sc, Y, Pd, Nb, V and, to a lesser extent, Ru and Rh. With increasing pressure, as long as there is no structural change, there is usually an increase in $\langle I^2 \rangle$ and $\langle \omega^2 \rangle$, while $N(0)$ decreases. Depending on the relative changes in these quantities T_c may increase or decrease. For Y, Sc, Pd, V, Nb and their alloys the suppression of spin fluctuations under pressure should be considered as well. Pressure dependence of T_c in Nb up to 132 GPa has been studied experimentally by Struzhkin *et al* [55]. Abrupt changes in T_c at 5 and 60 GPa have been explained via calculations by Tse *et al* [56] as being due to changes in the topology of the Fermi surface. The calculated values of λ_{ep} decrease rapidly with pressure (due to rapid increase in phonon frequencies) and then increase abruptly at a density, presumably corresponding to a pressure of ∼5 GPa due to a change in Fermi surface topology. Beyond this, the calculated λ_{ep} decreases again. Although the calculations explain the abrupt changes, and yield EP coupling constants in qualitative agreement with the experiment, the exact profile of the T_c versus pressure curve is not well reproduced. The experiments show an initial decrease in T_c followed by a sharp increase at ∼5 GPa. However, the initial drop in measured T_c is a lot less than the calculated EP coupling constants would suggest. Similarly, the rise in measured T_c immediately above 5 GPa is stronger than what is suggested by the calculated λ_{ep}. The inclusion of spin-fluctuation effects, strong at ambient pressure and diminishing with increasing pressure, can explain the discrepancy. In fact, the calculated λ_{ep} [56] decreases from 1.36 (in close agreement with 1.39, quoted in this work) to 1.02 as the pressure increases to 5 GPa, and then increases sharply to 1.21. The corresponding numbers obtained from

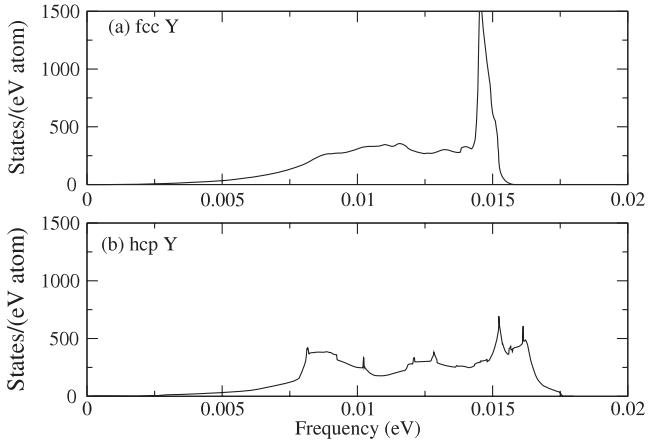

Figure 8. Phonon distribution in fcc and hcp phases of Y, with the density of the fcc phase chosen to be the same as the hcp ground state.

experiment [55] are 1.16, 1.12 and 1.18. The experimental numbers can be interpreted as $\sim \lambda_{ep}$–λ_{es}. This gives $\lambda_{es} = 0.2$ at ambient pressure, decreasing to 0.1 at 5 GPa and then to 0.03 above 5 GPa. Note that the value $\lambda_{es} = 0.2$ is not far from the value 0.126 quoted in table 5.

Finally, it seems reasonable to guess from the results for Sc and Y that the corresponding 5d metal La should also exhibit large spin fluctuations and the pressure dependence of its T_c [59] should be somewhat dictated by these effects. This idea is supported by the fact that La has the highest electronic specific heat constant among the 5d metals [38]. Pressure dependence of T_c in La has been studied experimentally by several groups [57–59]. The most recent study [59] quotes T_cs higher than the two previous reports [57, 58], and also reveals abrupt increases in T_c around 2 and 5.4 GPa, not seen previously. The recent work also extends the study to 50 GPa, higher than the previous works that were limited to less than 20 GPa [57]. A pseudopotential-based plane-wave basis calculation by Gao *et al* [60] for the fcc phase shows agreement, without any consideration of spin fluctuations, between the calculated T_cs at three pressures between 2.5 and 4.5 GPa and those measured in the earlier studies [57, 58]. A couple of comments are necessary at this point. Tissen *et al* [59] claim that the earlier measurements [57, 58] were for metastable fcc states. Their measured T_c s for the fcc phase are lower than those of the earlier measurements [57, 58], and also lower than the values calculated by Gao *et al* [60]. T_c, in the work by Gao *et al*, is calculated via the McMillan formula only. They use a pressure-independent Coulomb pseudopotential, which, fitted to T_c at one pressure, seems to work for the other two pressures as well. This work does not consider the ambient pressure (hcp or dhcp) case, where the spin-fluctuation effects should be most pronounced. It is conceivable that the spin-fluctuation effects in the fcc phase of La are lower (and perhaps negligible) than in the hcp or dhcp phases. Note that the idea that such effects should be significant in La are based on our study of the hcp phases of Sc and Y. Further work, both theoretical and experimental, is needed to resolve the issues of the discrepancies between the old and the recent measurements, as well as the role of spin fluctuations in La.

For superconducting alloys containing either Sc, Y, Nb, V and Pd, a lowering of T_c with increasing concentration of these elements should be observable. Jensen and Maita [61] attribute the rapid decrease in the T_c of Zr–Sc alloys with increasing Sc concentration to spin fluctuations. Rietschel *et al* [62] have argued that spin fluctuations are responsible for a stronger suppression of T_c in VN, compared with NbN. According to these authors T_c in VN, based solely on EP interaction, should be ∼30 K, in contrast to the observed value of 8.6 K. The alloy Pd–Ag is an interesting case. For some time it was believed that this alloy system should be superconducting for concentrations of Ag large enough to reduce the spin fluctuations, while the EP coupling still remains strong. Pd–Ag was never found to be superconducting [63]. This is consistent with our result that the EP coupling in Pd is sufficiently low to render it non-superconducting even without consideration of spin fluctuations. Addition of Ag lowers the EP coupling constant, making it less favourable to superconductivity. Note that claims of superconductivity in the Ag–Pd–Ag epitaxial metal film sandwich have been made [64]. Our results for bulk metals cannot be applied to such cases. Finally, these considerations should hold for amorphous (glassy) superconducting alloys as well [65–67].

6. Summary

We have studied the electron–phonon and electron–paramagnon interactions in 4d and nonmagnetic 3d transition metals, and some simple and noble metals. The electron–phonon coupling constants and Eliashberg spectral functions are calculated via a *first-principles* method. We study the trends, as a function of band filling, in the Fermi surface average of the electron–phonon scattering, phonon frequencies and the electron–phonon coupling constants. Wherever applicable, we provide a comparison of the *first-principles* linear response results with those based on the rigid muffin-tin approximation. Implications of the results for the pressure dependence of superconductivity and for alloys are discussed briefly. Our results support the Matthias rule of superconductivity [33], which asserts that for electron–phonon superconductivity in metallic systems the optimum conditions occur for 5 and 7 electrons/atom. We point out that spin fluctuations play an important role in suppressing superconductivity completely in Sc and Y, and partially in some of the metals at the start of the 3d and 4d series, and thus play an important role in the validity of the Matthias rule.

Acknowledgments

This work was supported by a grant from the Natural Sciences and Engineering Research Council of Canada. The author acknowledges helpful discussions with B Mitrović.

References

[1] McMillan W L 1968 *Phys. Rev.* **167** 331
[2] Dynes B and Varma C M 1976 *J. Phys. F: Met. Phys.* **6** L215
[3] Papaconstantopoulos D A, Boyer L L, Klein B M, Williams A R, Moruzzi V L and Janak J F 1977 *Phys. Rev.* B **15** 4221
[4] Kittel C 1996 *Introduction to Solid State Physics* 7th edn (New York: Wiley) table 3, chapter 3
[5] see, for example, Andersen O K, Jepsen O and Glötzel D 1985 *Highlights of Condensed Matter Theory* ed F Bassani *et al* (Amsterdam: North-Holland) p 148 (figure 25)
[6] Berk N F and Schrieffer J R 1966 *Phys. Rev. Lett.* **17** 433
[7] Pinski F J and Butler W H 1979 *Phys. Rev.* B **19** 6010
[8] Savrasov S Y and Savrasov D Y 1992 *Phys. Rev.* B **46** 12181
[9] Savrasov S Y 1996 *Phys. Rev.* B **54** 16470
[10] Savrasov S Y and Savrasov D Y 1996 *Phys. Rev.* B **54** 16487
[11] Schrieffer J R 1968 *J. Appl. Phys.* **39** 642
[12] Gaspari G D and Gyorffy B L 1972 *Phys. Rev. Lett.* **28** 801
[13] see, e.g. Terakura K and Ojala E J 1985 *J. Phys. F: Met. Phys.* **15** 2145 and references therein
[14] Allen P B and Mitrović B 1982 *Advances in Solid State Physics* vol 37 (New York: Academic) p 1
[15] Daams J M, Mitrović B and Carbotte J P 1981 *Phys. Rev. Lett.* **46** 65

[16] Schilling J S 2001 arXiv:cond-mat/0110267v1
Schilling J S 2007 arXiv:cond-mat/0703730v1
Schilling J S 2006 High pressure effects *Treatise on High Temperature Superconductivity* ed J R Schrieffer (New York: Springer) at press (arXiv:cond-mat/0604090v1)
[17] Garland J W and Bennemann K H 1972 *Superconductivity in d- and f-band Metals* ed D H Douglass (New York: American Institute of Physics) pp 255–92
[18] Morel P and Anderson P W 1962 *Phys. Rev.* **125** 1263
[19] see references and discussion in section V of Gunnarsson O 1997 *Rev. Mod. Phys.* **69** 575
[20] Lüders M *et al* 2005 *Phys. Rev.* B **72** 024545 and references therein
[21] MacDonald A H 1982 *Can. J. Phys.* **60** 710
[22] Bose S K 2008 *J. Phys.: Condens. Matter* **20** 045209
[23] Blöchl P E *et al* 1994 *Phys. Rev.* B **49** 16223
[24] Perdew J P and Wang Y 1992 *Phys. Rev.* B **45** 13244
[25] Perdew J P, Chevary J A, Vosko S H, Jackson K A, Pederson M R, Singh D J and Fiolhais C 1992 *Phys. Rev.* B **46** 6671
[26] Allen P B 1972 *Phys. Rev.* B **6** 2577
[27] Allen P B and Dynes R C 1975 *Phys. Rev.* B **12** 905
[28] see Dederichs P H, Schober H and Sellmyer D J (ed) 1981 *Metals: Phonon and Electron States and Fermi Surfaces* (*Springer Series Landöldt-Bernstein New Series 111/13a* K-H Hellwege and J L Olsen (ed)) (Berlin: Springer) and references therein
[29] Eichler A, Bohnen K-P, Reichardt W and Hafner J 1998 *Phys. Rev.* B **5** 324
[30] Kong Y, Dolgov O V, Jepsen O and Andersen O K 2001 *Phys. Rev.* B **64** 020501
[31] Glötzel D, Rainer D and Schober H R 1979 *Z. Phys.* B **35** 317
[32] Skriver H L and Mertig I 1985 *Phys. Rev.* B **32** 4431
Skriver H L and Mertig I 1990 *Phys. Rev.* B **41** 6553
[33] Matthias B T 1955 *Phys. Rev.* **97** 74
[34] Bose S K, Dolgov O V, Kortus J, Jepsen O and Andersen O K 2003 *Phys. Rev.* B **67** 214518
[35] Bose S K, Kato T and Jepsen O 2005 *Phys. Rev.* B **72** 184509
[36] Wittig J, Probst C, Schmidt F A and Gschneidner K A Jr 1979 *Phys. Rev. Lett.* **42** 469
[37] Janak J F 1977 *Phys. Rev.* B **16** 255
[38] See table XIII and figure 18 of Gschneidner K A Jr 1964 *Solid State Physics* vol 16, ed F Seitz and D Turnbull (New York: Academic) pp 275–426
[39] Rietschel H and Winter H 1979 *Phys. Rev. Lett.* **43** 1256
[40] Mazin I I, Papaconstantopoulos D A and Mehl M J 2002 *Phys. Rev.* B **65** 100511(R)
[41] Capellmann H 1970 *J. Low Temp. Phys.* **3** 189
[42] Das S G 1976 *Phys. Rev.* B **13** 3978
[43] MacDonald A H, Liu K L and Vosko S H 1977 *Phys. Rev.* B **16** 777
[44] Thakor V, Staunton J B, Poulter J, Ostanin S, Ginatempo B and Bruno E 2003 *Phys. Rev.* B **68** 134412
[45] Rath J and Freeman A J 1975 *Phys. Rev.* B **11** 2109
[46] Liu S, Gupta R P and Sinha S K 1971 *Phys. Rev.* B **4** 1100
[47] Crowe S J, Dugadale S B, Major Zs, Alam M A, Duffy J A and Palmer S B 2004 *Europhys. Lett.* **65** 235
[48] Dreyssé H and Demangeat C 1997 *Surf. Sci. Rep.* **28** 65–122
[49] Pfandzeller R, Steierl G and Rau C 1995 *Phys. Rev. Lett.* **74** 3467
[50] Steierl G, Pfandzeller R and Rau C 1994 *J. Appl. Phys.* **76** 6431
[51] Krüger P, Demangeat C, Parlebas J C and Mokrani A 1996 *Mater. Sci. Eng.* B **37** 242
[52] Hamlin J J and Schilling J S 2007 *Phys. Rev.* B **76** 012505
see also Hamlin J J and Schilling J S 2007 arXiv:cond-mat/0703730v1
[53] Hamlin J J, Tiessen V G and Schilling J S 2006 *Phys. Rev.* B **73** 094522
[54] Yin Z P, Savrasov S Y and Pickett W E 2006 arXiv:cond-mat/0606538v1
[55] Struzhkin V V, Timofeev Y A, Hemley R J and Mao H-K 1997 *Phys. Rev. Lett.* **79** 4262
[56] Tse J S, Li Z, Uehara K, Ma Y and Ahuja R 2004 *Phys. Rev.* B **69** 132101
[57] Balster H and Wittig J 1975 *J. Low Temp. Phys.* **21** 377
[58] Smith T F and Gardner W E 1966 *Phys. Rev.* **146** 291
[59] Tissen V G, Ponyatovskii E G, Nefedova M V, Porsch F and Holzapfel W B 1996 *Phys. Rev.* B **53** 8238
[60] Gao G Y *et al* 2007 *J. Phys.: Condens. Matter* **19** 425234
[61] Jensen M A and Maita J P 1966 *Phys. Rev.* **149** 409
[62] Rietschel H, Winter H and Reichardt W 1980 *Phys. Rev.* B **22** 4284
[63] Schuller I K, Hinks D and Soulen R J Jr 1982 *Phys. Rev.* B **25** 1981
[64] Brodsky M B 1982 *Phys. Rev.* B **25** 6060
[65] Hamed F, Razavi F S, Bose S K and Startseva T 1995 *Phys. Rev.* B **52** 9674
[66] Hamed F, Razavi F S, Zaleski H and Bose S K 1991 *Phys. Rev.* B **43** 3649
[67] Bose S K, Kudrnovský J, Razavi F S and Andersen O K 1991 *Phys. Rev.* B **43** 110